


Emergent normal-state Mottness in the infinite-layer NdNiO₂ superconductorL. Craco,^{1,*} A. S. de Arruda,^{1,†} and S. Leoni^{2,‡}¹*Institute of Physics, Federal University of Mato Grosso, 78060-900 Cuiabá, Mato Grosso, Brazil*²*School of Chemistry, Cardiff University, Cardiff CF10 3AT, United Kingdom* (Received 12 May 2022; revised 12 July 2022; accepted 1 September 2022; published 17 October 2022)

We present a computational study based on density functional plus dynamical mean-field theory calculations for the normal-state electronic reconstruction of pure and hole-doped NdNiO₂ superconductors. Our results capture the T dependence of the electrical resistivity, providing a many-particle interpretation of the emergence of pseudogaplike features at low energies as well as the weakly insulating regime seen in experiment. We show how Mottness manifests itself in the weak localization to bad-metallicity crossover due to strong correlation in the e_g -shell one-particle spectral functions and self-energies.

DOI: [10.1103/PhysRevResearch.4.043036](https://doi.org/10.1103/PhysRevResearch.4.043036)

I. INTRODUCTION

The discovery of superconductivity in Sr-doped NdNiO₂ thin films [1] marks the nickel age of superconductivity [2]. After a host of experimental and theoretical efforts, this family of layer superconductors now includes a range of hole-doped systems [3,4], Pr or La and other rare-earth ions in place of Nd [5–8], and the quintuple-layer system Nd₆Ni₅O₁₂ [9], among other higher-order layered systems [10]. As for the cuprates, the basic structural element in the infinite-layer nickelates is the NiO₂ square lattice [2]; see Fig. 1. A number of theory studies indicate that orbital degrees of freedom [11–13] and electronic correlations are relevant in this material class [14], and hence a fundamental question in this field is whether orbital selectivity and Mott-Hubbard physics play any role in determining the electronic state that might host unconventional superconductivity coexisting with intrinsic magnetism arising from Mottness [15,16]. Although magnetic impurities might be present in the real solid [17], a recent muon spin rotation-relaxation study [18] reports an intrinsic magnetic ground state, regardless of the rare-earth ion or doping concentration which arises from local moments on the Ni sublattice [18]. Importantly, the coexistence of magnetism with superconductivity suggests an underlying physics with similarities akin to some Fe superconductors [19], which might be qualitatively distinct from the doped cuprates [20], prompting the question, To what extent are nickelates and cuprates similar [21,22]? Here, we shed light on this problem, showing that the paramagnetic normal state of the NdNiO₂ parent compound is in close proximity to Mott localization.

We unearth the important role played by two-orbital electron-electron interactions [11,12,23] in the e_g shell of pure and hole-doped NdNiO₂.

The $3d^9$ nickelates (Ni¹⁺ nominal state) such as NdNiO₂ have long been considered in the context of divalent $3d^9$ cuprates (Cu²⁺) [22,24]. Despite being isostructural to the (Sr,Ca)CuO₂ compound, it remains unclear how similar these two superconducting families really are. Notable here is the recent cluster dynamical mean-field theory (DMFT) study on *minimal models* for NdNiO₂ and CaCuO₂ systems [25], which shows that the stoichiometric compounds are antiferromagnetically ordered. Moreover, according to this study, at low doping, superconductivity in both materials is limited by competition with long-range antiferromagnetic order, and superconductivity emerges at around the same hole doping for both compounds. It is worth noting, however, that the cuprates are charge-transfer insulators instead of being at the verge of Mott localization as in some Fe superconductors [19,26], and doped holes appear in the oxygen p band while Cu is retained almost in its $3d^9$ character with the concomitant formation of the Zhang-Rice singlet [27]. Finally, in infinite-layer Ni superconductors, there is a large pd -band gap so the system might be closer to Mottness [28], and holes would reside more predominantly in the Ni $3d$ bands [15,29], similar to Fe-based superconductors [19].

Also noteworthy for infinite-layer nickelates are the resistivity upturn near 50–70 K in the parent compounds and the normal-state resistivity which is approximately linear in temperature T before approaching the superconducting phase transition [1,15,30] as well as the T dependence of the Hall coefficient. The doped infinite-layer nickelates possess Hall coefficients that, while sensitive to factors such as doping concentration [3,4,31,32], thickness [33], and cation composition [7,31], remain negative at all temperatures or exhibit a zero crossing. This seems to suggest a two-band picture with substantial electron- and hole-pocket contributions [8,29,34]. It should be noted that attention has been given to the multiband character of NdNiO₂: In the paramagnetic normal state, in addition to the Ni- $d_{x^2-y^2}$ band, the Nd- $5d$ states also cross the Fermi level, E_F . The latter leads to the appearance of electron

*lcraco@fisica.ufmt.br

†aarruda@fisica.ufmt.br

‡LeoniS@cardiff.ac.uk

pockets at the Γ and A points, with mainly Nd- d_{z^2} and Nd- d_{xy} orbital character, respectively. These electron pockets give rise to self-doping of the large holelike Ni- $d_{x^2-y^2}$ Fermi surface [10,22,34,35]. However, the mixing between Ni and Nd states is small, leading to bands with a single orbital characteristic [34]. Thus, since we are mainly interested in the electronic structure reconstruction upon hole-doping the NdNiO₂ parent compound, in this paper we will focus on a two-orbital model composed of Ni- $x^2 - y^2$ and Ni- z^2 electronic states [11,12,23]. As shown below, this two-orbital model treated within the density functional plus dynamical mean-field theory (DFT+DMFT) [36] correctly describes the evolution of the weakly insulating state [2] towards a strange bad metal with nearly linear T dependence of the electrical resistivity as seen in experiments for Sr-doped NdNiO₂ films [1,15].

II. THEORY AND RESULTS

It is now recognized that the electronic properties of infinite-layer nickelates are determined by the complex interplay between different factors, including the on-site Coulomb repulsion ($3.0 \leq U \leq 10$ eV) [11–13,22,29] and the Hund's interaction ($0.7 \leq J_H \leq 1.0$ eV) [12,13,16] as well as multiband and multiorbital degrees of freedom [8,11–13,16,29]. Based on DFT calculations [12], the one-electron Hamiltonian relevant to multiple-layer nickelates is $H_0 = \sum_{\mathbf{k},a,\sigma} \epsilon_a(\mathbf{k}) c_{\mathbf{k},a,\sigma}^\dagger c_{\mathbf{k},a,\sigma} + \sum_{i,a,\sigma} \epsilon_a^{(0)} n_{i,a,\sigma}$, where $a = x^2 - y^2, z^2$ denotes its e_g orbitals. $\epsilon_a(\mathbf{k})$ is the one-electron band dispersion, which encodes details of the one-electron (DFT) band structure [12], and the $\epsilon_a^{(0)}$ are the corresponding on-site orbital energies, whose bare values are read off from the orbital-resolved DFT spectral functions. These e_g orbitals are the relevant one-particle inputs for two-orbital DMFT, which generates a weakly insulating electronic state in close proximity to Mott localization, as shown below. Neglecting the Nd-5d states at the one-particle level [11,12,23], the correlated many-body Hamiltonian relevant to NdNiO₂ and analogs reads $H_{\text{int}} = U \sum_{i,a} n_{i,a,\uparrow} n_{i,a,\downarrow} + U' \sum_{i,a \neq b} n_{i,a} n_{i,b} - J_H \sum_{i,a \neq b} \mathbf{S}_{i,a} \cdot \mathbf{S}_{i,b}$. Here, $U' = U - 2J_H$ is the interorbital Coulomb interaction term. We evaluate the many-particle Green's functions [$G_{a,\sigma}(\omega)$] of the two-orbital Hamiltonian $H = H_0 + H_{\text{int}}$ using the two-orbital iterated perturbation theory as impurity solver [37]. This real frequency perturbative *ansatz* has a proven record of good semiquantitative agreement with experiment for a range of correlated materials, and it gives results in qualitative accord with continuous-time quantum Monte Carlo (CT-QMC) calculations for correlated multiorbital (MO) systems [38].

A detailed understanding of the electronic structure of correlated electron systems requires special methods and numerical tools, for example, the continuous-time hybridization algorithm and the constrained random phase approximation applied in Ref. [12]. The DFT+DMFT approximation takes inputs from DFT, such as the orbitally projected density of states (DOS) or the energy bands, the on-site energies, and the crystal field splittings. Figure 2 shows the orbitally projected DOS derived in Ref. [12] (see Ref. [39]), which is used here as input to two-orbital DMFT calculations. Similar to Ref. [12], the Green's functions are calculated using the single-site DMFT approximation in which only the site-local

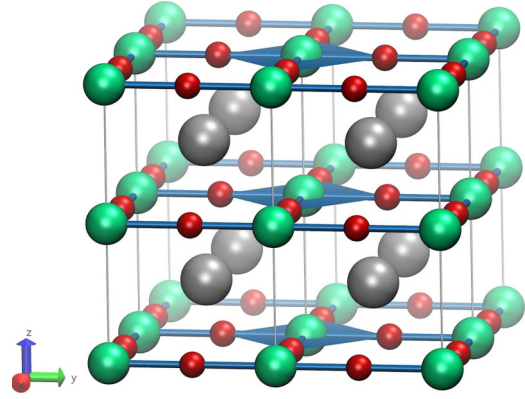


FIG. 1. Tetragonal (space group $I4/mmm$) crystal structure of NdNiO₂. Infinite NiO₂ square lattices are stacked along the c axis, with Ni in square planar coordination (blue squares). Nd is gray, Ni is green, and O is red. Ni-O bonds (blue) are highlighted. Eight conventional unit cells are shown.

matrix elements of the self-energy between correlated orbitals are retained. As seen, the $x^2 - y^2$ spectral function displays two peaks: one at 0.37 eV below E_F and the second one at 6.0 eV binding energy reflecting the hybridization of Ni- $d_{x^2-y^2}$ and O-2p states, which divides the $x^2 - y^2$ spectra into bonding and antibonding portions. For the z^2 orbital sector, the

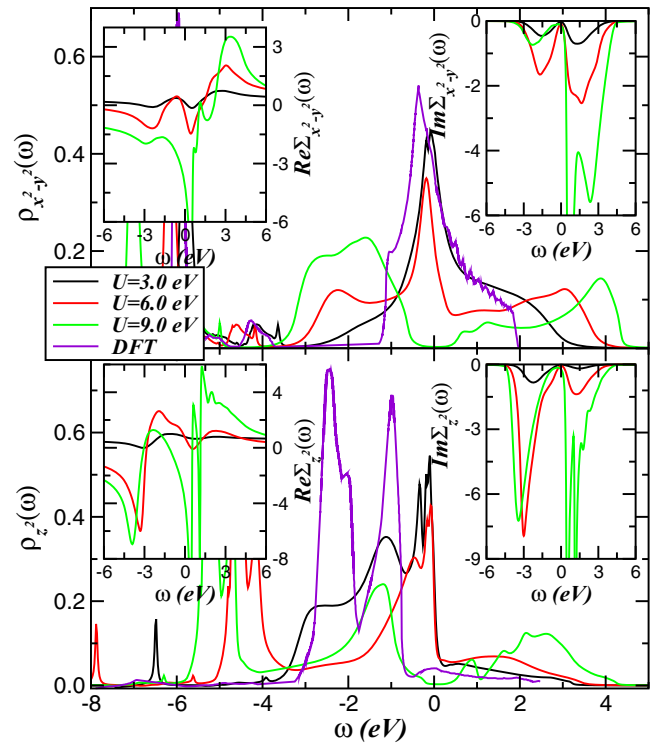


FIG. 2. Evolution of the e_g spectral functions of NdNiO₂ for three different U values and fixed $J_H = 0.75$ eV. The bare (DFT) density of states (DOS) [12] is shown for comparison. Notice the electronic reconstruction due to sizable two-orbital correlations and the downshift of the z^2 orbital. Insets show the evolution of the self-energy real (left) and imaginary (right) parts with increasing U .

different methods used in Ref. [12] predict slightly different Ni-3d weights in the bonding region; however, in all cases the spectral function for the z^2 orbital shows nearly one-dimensional orbital character with sharp peaks at -2.4 and -0.98 eV, as visible in Fig. 2. Interesting as well is the fact that this orbital component is not hybridized with the O-2p bands but with the Nd-5d states lying above Fermi energy, resulting in a weak tail at energies above E_F . From a general perspective, the emergence of z^2 electronic states above E_F compensate to some extent self-doping effects arising from the hybridization between Nd-5d conduction electrons and Ni-3d valence bands [29,41,42]. How the $x^2 - y^2$ and z^2 DFT spectral functions of NdNiO₂ are reshaped by two-orbital dynamical correlations [11,12,23] and hole doping is our focus below.

Let us now present our DFT+DMFT results. In Fig. 2 we show how the orbital-resolved spectral functions of NdNiO₂ obtained for three different U values and fixed $J_H = 0.75$ eV are reshaped as compared with the bare DFT DOS. As seen, at $U = 3.0$ eV the shape of the $x^2 - y^2$ DFT DOS is partially retained while the z^2 spectra are shifted towards E_F (see our discussion below). However, in good qualitative accord with earlier calculations [12,13], lower and upper Hubbard bands (LHBs and UHBs, respectively) emerge in the correlated electronic structure of NdNiO₂. On increasing the on-site U , these incoherent electronic states are transferred to higher energies with the concomitant narrowing of the Kondo-quasiparticle resonances [43] at low energies near E_F . Finally, at the critical $U_c = 9.0$ eV, NdNiO₂ is in the Mott side of the correlated phase diagram [44], with a Mott-Hubbard gap emerging across E_F . Future photoemission spectroscopy studies are called for to corroborate our prediction of an emergent Mott localized electronic state in strained infinite-layer nickelates, where the U/W ratio (W is the bare one-particle bandwidth) is expected to increase in the real solid [44].

To further prove the correlated electronic structure reconstruction of NdNiO₂, in the insets of Fig. 2 we show the frequency dependence of the self-energy $[\Sigma_a(\omega)]$ imaginary (right panels) and real (left panels) parts; the latter determines the quasiparticle mass enhancement [12,13]. From our results, it is evident that $\Sigma_{z^2}(\omega)$ for $U \geq 6.0$ eV has larger values at negative frequencies as compared with the $x^2 - y^2$ orbital, yielding incoherent electronic excitations and causing the formation of local moments (LHBs). In the metallic regime, our DFT+DMFT results reveal a quadratic-in-energy dependency characteristic of Landau-Fermi liquid (LFL) metals [43] in $\text{Im}\Sigma_a(\omega)$ at low frequencies. The real part of the self-energy $[\text{Re}\Sigma_a(\omega)]$ also displays the characteristic linear LFL behavior at low energies. At U_c the self-energies show strong particle-hole asymmetry and a diverging ω dependence responsible for Mott localization. Finally, our results in Fig. 2 show that orbital differentiation in NdNiO₂ is reflected in the self-energies. The z^2 orbital shows much stronger correlations below E_F than the $x^2 - y^2$ one, with higher local moments and steeper slope in $\text{Re}\Sigma_a(\omega)$.

It is worth noting here that the appearance of stronger electronic correlations in the z^2 orbital as compared with the $x^2 - y^2$ orbitals remains rather counterintuitive since the former is almost fully occupied in the bare one-band picture.

Normally, for the one-band Hubbard model, electrons are rather weakly correlated in systems far from half filling. However, this canonical understanding does not hold completely true for MO systems with sizable interorbital correlations [45]. As a result, the effective band filling combined with two-orbital Hartree shifts leads to charge flow from the $x^2 - y^2$ orbital to the z^2 orbital, in analogy with that reported for a spin-polarized ferromagnetic system where the valence band DOS of the majority spin channel is shifted towards E_F [45] while the less polarized channel is barely affected [45,46]. Also relevant to NdNiO₂ is the fact that the $x^2 - y^2$ orbital has a larger bandwidth as compared with the z^2 orbital, implying a reduced U/W ratio. Moreover, the intensity of the Van Hove singular peaks which are shifted towards E_F is higher for the z^2 orbital as compared with the $x^2 - y^2$ orbital. In this situation, sizable interorbital Coulomb correlation effects induced by U' will promote an extended Van Hove singularity regime similar to that discussed, for example, for doped graphene [47] and Sr₂RuO₄ [48]. We shall mention here that in low-dimensional systems the DOS diverges and the excess of charge carriers enhances intrinsic electronic correlations [49], an effect which is now commonly referred to as an extended Van Hove singularity [47]. Accordingly, our results in Fig. 2 indicate that strong electronic correlations in the z^2 orbital of the NdNiO₂ parent compound result from interplay between orbital polarization and the proximity of its Van Hove singularity to E_F . This is the key step, which allows us to understand the two-orbital electronic reconstruction in this system.

To characterize the Mott localized [44] as well as the pseudogap regime [26] in NdNiO₂, in Fig. 3 we show its orbital-resolved DOS at the border of the first-order Mott metal-insulator transition, which according to our theory takes place at $U_c = 9.0$ eV. Interestingly, this value is consistent with extant theoretical results where at a reasonable large interaction strength $U = 10$ eV the e_g orbital sector is Mott insulating [50]. More importantly, in Fig. 3 we show that pseudogapped (V -shaped) spectral functions near E_F emerge in the incoherent metallic regime of NdNiO₂. Upon reducing the strength of the on-site Coulomb interaction U , the pseudogap phase evolves towards an electronic state with asymmetric Kondo quasiparticles [43]; see our results for $U = 8.0$ eV. However, if our proposal is to hold, the critical metal at the border of the Mott transition in NdNiO₂ should be characterized by pseudogapped electronic states at low energies, and future experiments [26] on samples free from extended defects [30] could verify this aspect. As seen, the DFT+DMFT electronic structure in Fig. 3 shows large-scale changes in spectral weight transfer (SWT) below the critical phase boundary. As shown in Fig. 3, the relatively large range of the V -shaped pseudogap spectrum is closely related to the frequency dependence of the self-energy imaginary parts, which show deviations from the ω^2 dependence of canonical LFL metals [43]. Below the Mott transition only our results for $U = 8$ eV show characteristic LFL-like features, while close to Mottness the self-energies display sublinear ω dependence of power-law liquids [51]. Similar self-energy behavior to that shown later in Fig. 5, with sublinear energy dependence, was also found in Fe-based superconductors [52,53], suggesting a common scenario of correlation-induced

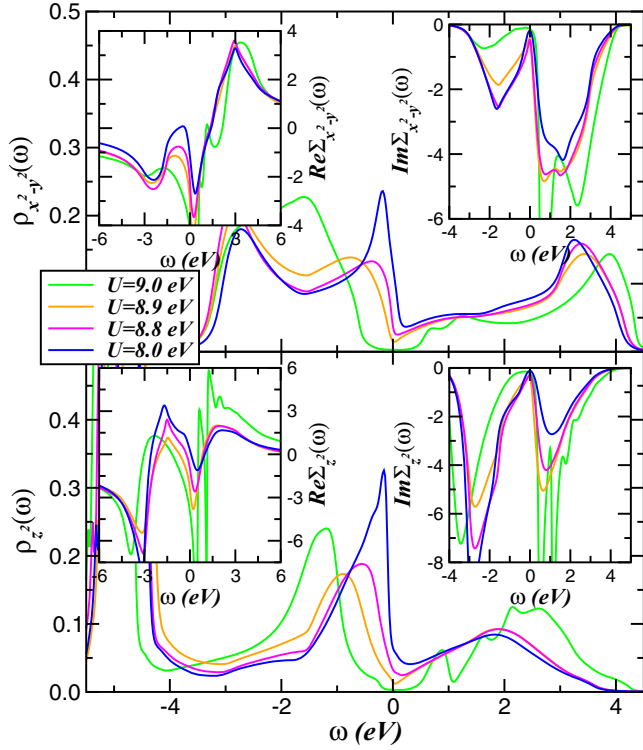


FIG. 3. Electronic reconstruction near Mott localization in NdNiO₂. Notice the first-order phase transition from a Mott insulator to a pseudogap metal. Insets display the frequency dependence of the self-energy imaginary and real parts, showing considerable changes across the Mott transition.

multiorbital electronic reconstruction in correlated superconducting materials.

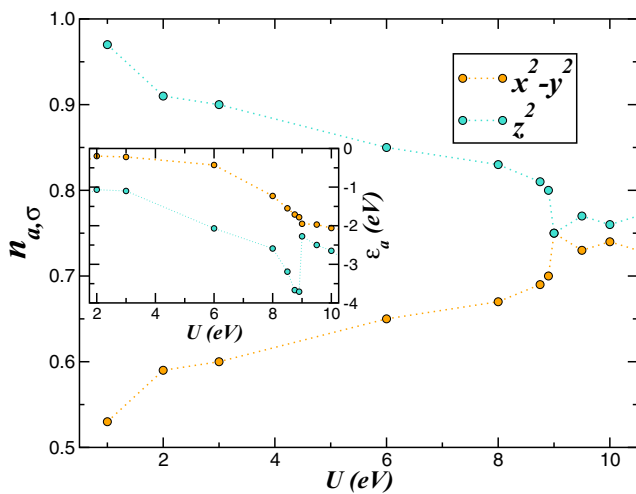


FIG. 4. e_g orbital occupancies as a function of the on-site U . Notice the reduction of the orbital polarization upon increasing U and its suppression at $U_c = 9.0$ eV. The inset shows the evolution of the on-site orbital energies ϵ_a as a function of U . An important feature to be seen is the sudden reduction of ϵ_{z^2} at the Mott transition.

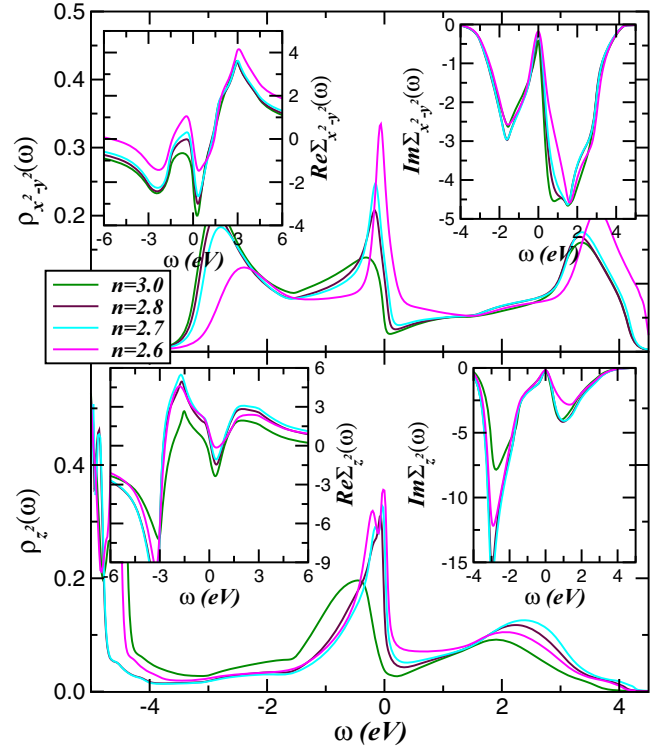


FIG. 5. Effect of hole-doping the NdNiO₂ parent compound on the e_g spectral functions (main panels) and self-energies (insets) computed using $U = 8.75$ eV. Particular features to be seen are the large spectral weight transfer and the orbital differentiation at low energies upon small changes in the total band filling n .

For the sake of completeness, in Fig. 4 we display the orbital occupation $n_{a,\sigma}$, computed using the orbital-resolved spectral functions of the two-orbital Hubbard model for NdNiO₂. As in Ref. [54] we observe clear changes in orbital polarization, particularly at energies close to U_c . These responses are characteristic of strongly correlated systems, where the changes in the orbital occupation are linked to dynamical fluctuations in the reconstructed electronic state. Notably, orbital polarization is reduced approaching U_c , driving continuous changes in the correlated spectral functions as in Fig. 3. Our results in Fig. 4 imply a continuous reduction of ferro-orbital order due to a U' -induced, strong interorbital proximity effect with the spectral weight below U_c being continuously removed from the z^2 orbital sector and transferred to the $x^2 - y^2$ orbital sector in spite of the spin state [55]. Also interesting are our results in the inset of Fig. 4, showing the evolution of the on-site orbital energies ϵ_a , or the center of gravity of the correlated spectral functions, as a function of U . As seen, with increasing U , DFT+DMFT severely renormalizes the center of gravity of each orbital promoting changes in the correlated spectral functions as displayed in Figs. 2 and 3. This fact, generic to MO systems, is an interesting manifestation of correlation-induced orbital rearrangement and controls the changes in the correlated electronic spectra across the Mott transition. Due to particle-hole asymmetry and anisotropic DFT one-particle energies and hoppings, two-orbital correlations renormalize the e_g orbitals

of NdNiO₂ in different ways, leading to intrinsic orbital selectivity [36,56]. Within DFT+DMFT, this orbital-selective mechanism involves two renormalizations: Static (two-orbital Hartree) renormalization shifts the e_g bands relative to each other by amounts that depend on their bare on-site orbital energies and occupations. In addition, dynamical effects of U and U' drive large SWT over wide energy scales [56]. This result implies that in correlated electron systems, small variations of on-site U drive appreciable SWT, producing orbital-selective renormalizations of the on-site energies. As seen in Fig. 5, near the Mott transition the z^2 orbital is the most severely affected. At the critical $U_c = 9.0$ eV we observe an abrupt reduction of ϵ_{z^2} , while $\epsilon_{x^2-y^2}$ remains nearly unchanged across the Mott metal-insulator transition.

To get more insights into the normal-state electronic structure reconstruction of NdNiO₂, we now focus on the effect of hole-doping the parent compound. Even though no experimental data exist, the generic appearance of novel electronic states in a wide variety of other correlated electron systems makes this an important question to inquire into. Our aim here is to build upon the strengths of correlated electronic structure modeling to introduce additional dynamical SWT via hole doping within the range relevant to experiments [2]. As seen in Fig. 5, our results for fixed $U = 8.75$ eV and $J_H = 0.75$ eV [57] confirm that metallicity is enhanced upon hole-doping the pseudogapped parent compound [1,9,15]. This is tied to the fact that the Kondo-quasiparticle resonance is shifted towards E_F upon doping. An intriguing observation, however, is the change in the orbital-selective SWT induced by doping with an orbital-dependent narrowing of the Kondo-quasiparticle peak and the partial SWT from the valence band to the UHBs. What is the origin of these orbital-selective features? In correlated electron systems such as NdNiO₂, scattering between different carriers in orbital states leads to two main effects: an orbital-dependent shift of the e_g bands relative to each other via static-Hartree contributions (from the static part of the orbital-dependent self-energies), and strong dynamical correlations due to sizable U , U' , and J_H which cause appreciable SWT over large energy scales upon carrier doping. Thus, for hole-doped NdNiO₂, coexisting Kondo-quasiparticle components with a distinct electronic line shape should be visible at low energies, in spite of large-scale SWT induced by strong electron-electron interactions. These are stringent tests of our proposal, and experimental verification should place it on solid grounds.

Finally, in Fig. 6 we show the T dependence of the electrical resistivity $\rho(T)$ computed using the orbital-resolved DFT+DMFT spectral functions of pure and hole-doped NdNiO₂ for $U = 8.75$ eV and $J_H = 0.75$ eV [58]. As seen in the main panel of Fig. 6, the DFT+DMFT result for the NdNiO₂ parent compound shows a resistivity upturn below 100 K, a fingerprint of the weakly insulating state reported in the literature [2]. While in experiments the resistivity upturn is found to be below about 50–70 K [1,15,30], our results in Fig. 6 are in good qualitative accord with those reported for Nd₆Ni₅O₁₆ [9], where the insulating upturn sets in close to 150 K. Interestingly, upon hole doping the resistivity upturn is shifted to low T , until it disappears for a total e_g electron band filling of $n = 2.7$. At small hole doping ($n = 2.9$) the resistivity shows the “S”-like shape characteristic of a pseu-

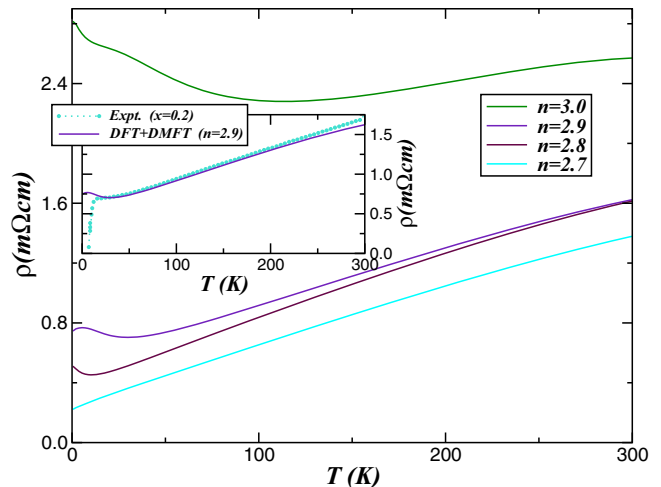


FIG. 6. Resistivity vs temperature (normalized to the $\rho(T)$ of the Nd_{0.8}Sr_{0.2}NiO₂ [1] superconductor) for pure and hole-doped NdNiO₂ obtained using the DFT+DMFT spectral functions for fixed $U = 8.75$ eV and different total occupancies n . Notice the insulating upturn in the resistivity of the stoichiometric compound and the “S”-like shape for $n = 2.9$. This suggests a pseudogapped metal similar to an FeSe superconductor [59]. Inset: Theory-experiment comparison of $\rho(T)$ for a hole-doped NdNiO₂ superconductor. Notice the quasi-linear T dependence of the transport data above 35 K in experiment [1], which is qualitatively reproduced by DFT+DMFT.

dogapped metal similar to Fe-based superconductors [53,59]. Moreover, for $n = 2.8$ the “S”-like form of $\rho(T)$ is smoothly suppressed, and only a tiny insulating upturn similar to those reported in Refs. [4,5] is visible below $T \simeq 10$ K. Finally, for $n = 2.7$, $\rho(T) \simeq T$ at low T , and the Fermi-liquid-like (FL-like) T^2 form is not observed upon partially hole-doping the parent compound. The underlying reason for this behavior is that at large U , U' , the moderately non-FL behavior is not destabilized by hole doping. Thus, with decreasing total electron concentration of the e_g shell, $\rho(T)$ becomes less weakly insulating, smoothly going over to a bad-metallic state at low temperatures [1,9,15]. In reality, as seen in the inset of Fig. 6, in superconducting NdNiO₂ an unconventional superconducting transition cuts off the low- T crossover to a pseudogap metal, but the overall T dependence of the DFT+DMFT resistivity in the normal state resembles that reported in experiment [15], where the normal-state resistivity is approximately linear with temperature before approaching the superconducting transition.

III. CONCLUSION

To summarize, we have used DFT+DMFT for a two-orbital Hubbard model to derive a correlation-induced electronic reconstruction in infinite-layer nickelates. In particular, considering NdNiO₂ as a suitable template, we have analyzed its paramagnetic weakly insulating and metallic behavior, unraveling it as an effect of two-orbital dynamical correlations. Also interesting is the orbital-selective electronic behavior obtained at the border of the Mott metal-insulator transition, where pseudogapped electronic excitations emerge at

low energies. As shown here, this arises from charge-carrier scatterings due to interplay between two-orbital polarization and electron-electron interactions, and this could be tested by a combination of spectral and transport measurements on bad-metallic samples. Such studies are called for, and should corroborate our proposal of two-orbital normal-state Mottness in infinite-layer NdNiO₂ [1,15] and related compounds [9]. Whether quantum criticality associated with a first-order Mott transition in conjunction with the development of a non-LFL metal [60] will be confirmed in infinite-layer nickelates is in our view of great interest. Our work provides a motivation to consider closer similarities between hole-doped NdNiO₂ and the Fe-chalcogenide superconductors. As in some Fe-chalcogenide systems, superconductivity in NdNiO₂ manifests as an instability of an anomalous bad metal. Based on a theory-experiment comparison we suggest that NdNiO₂ is an ideal candidate for testing this and the idea of strain-induced electronic localization in the Ni superconductors. Our findings thus provide a compelling motivation to consider these systems at the border of the Mott transition and suggest

a promising route to understand the pseudogaplike behavior [26] as well as the Mottness collapse without metallization [61] in non-LFL liquid materials.

Information on the data underpinning the results presented here, including how to access them, can be found in the Cardiff University data catalogue [62].

ACKNOWLEDGMENTS

L.C. and A.S.d.A. acknowledge CNPq and CAPES. S.L. thanks the Leverhulme Trust under Project No. RPG-2020-052. This work used the Isambard 2 UK National Tier-2 high-performance computing (HPC) service [63] operated by GW4 and the UK Meteorological Office and funded by EPSRC (EP/T022078/1 and EP/W03218X/1). S.L. also acknowledges the support of the Supercomputing Wales project (ARCCA), which is partly funded by the European Regional Development Fund (ERDF) via the Welsh Government.

-
- [1] D. Li, K. Lee, B. Y. Wang, M. Osada, S. Crossley, H. R. Lee, Y. Cui, Y. Hikita, and H. Y. Hwang, Superconductivity in an infinite-layer nickelate, *Nature (London)* **572**, 624 (2019).
- [2] Y. Ji, J. Liu, L. Li, and Z. Liao, Superconductivity in infinite layer nickelates, *J. Appl. Phys.* **130**, 060901 (2021); X. Zhou, P. Qin, Z. Feng, H. Yan, X. Wang, H. Chen, Z. Meng, and Z. Liu, Experimental progress on the emergent infinite-layer Ni-based superconductors, *Mater. Today* **55**, 170 (2022).
- [3] D. Li, B. Y. Wang, K. Lee, S. P. Harvey, M. Osada, B. H. Goodge, L. F. Kourkoutis, and H. Y. Hwang, Superconducting Dome in Nd_{1-x}Sr_xNiO₂ Infinite Layer Films, *Phys. Rev. Lett.* **125**, 027001 (2020).
- [4] S. Zeng, C. S. Tang, X. Yin, C. Li, M. Li, Z. Huang, J. Hu, W. Liu, G. J. Omar, H. Jani, Z. S. Lim, K. Han, D. Wan, P. Yang, S. J. Pennycook, A. T. Wee, and A. Ariando, Phase Diagram and Superconducting Dome of Infinite-Layer Nd_{1-x}Sr_xNiO₂ Thin Films, *Phys. Rev. Lett.* **125**, 147003 (2020).
- [5] M. Osada, B. Y. Wang, B. H. Goodge, S. P. Harvey, K. Lee, D. Li, L. F. Kourkoutis, and H. Y. Hwang, Nickelate superconductivity without rare-earth magnetism: (La, Sr)NiO₂, *Adv. Mater.* **33**, 2104083 (2021).
- [6] X. Chen, H. Zheng, D. P. Phelan, H. Zheng, S. H. Lapidus, M. J. Krogstad, R. Osborn, S. Rosenkranz, and J. F. Mitchell, Competing charge/spin-stripe and correlated metal phases in trilayer nickelates (Pr_{1-x}La_x)₄Ni₃O₈, *Chem. Mater.* **34**, 4560 (2022).
- [7] S. W. Zeng, C. J. Li, L. E. Chow, Y. Cao, Z. T. Zhang, C. S. Tang, X. M. Yin, Z. S. Lim, J. X. Hu, P. Yang, and A. Ariando, Superconductivity in infinite-layer nickelate La_{1-x}Ca_xNiO₂ thin films, *Sci. Adv.* **8**, eabl9927 (2022).
- [8] E. Been, W.-S. Lee, H. Y. Hwang, Y. Cui, J. Zaanen, T. Devereaux, B. Moritz, and C. Jia, Electronic Structure Trends Across the Rare-Earth Series in Superconducting Infinite-Layer Nickelates, *Phys. Rev. X* **11**, 011050 (2021).
- [9] G. A. Pan, D. F. Segedin, H. Labollita, Q. Song, E. M. Nica, B. H. Goodge, A. T. Pierce, S. Doyle, S. Novakov, D. C. Carrizales, A. T. N. Diaye, P. Shafer, H. Paik, J. T. Heron, J. A. Mason, A. Yacoby, L. F. Kourkoutis, O. Erten, C. M. Brooks, A. S. Botana *et al.*, Superconductivity in a quintuple-layer square-planar nickelate, *Nat. Mater.* **21**, 160 (2022).
- [10] H. LaBollita and A. S. Botana, Electronic structure and magnetic properties of higher-order layered nickelates: La_{n+1}Ni_nO_{2n+2} ($n = 4-6$), *Phys. Rev. B* **104**, 035148 (2021); M.-C. Jung, J. Kapeghian, C. Hanson, B. Pamuk, and A. S. Botana, Electronic structure of higher-order Ruddlesden-Popper nickelates, *ibid.* **105**, 085150 (2022).
- [11] F. Lechermann, Multiorbital Processes Rule the Nd_{1-x}Sr_xNiO₂ Normal State, *Phys. Rev. X* **10**, 041002 (2020).
- [12] J. Karp, A. Hampel, and A. J. Millis, Dependence of DFT+DMFT results on the construction of the correlated orbitals, *Phys. Rev. B* **103**, 195101 (2021).
- [13] See also P. Werner and S. Hoshino, Nickelate superconductors: Multiorbital nature and spin freezing, *Phys. Rev. B* **101**, 041104(R) (2020); P. Adhikary, S. Bandyopadhyay, T. Das, I. Dasgupta, and T. Saha-Dasgupta, Orbital-selective superconductivity in a two-band model of infinite-layer nickelates, *ibid.* **102**, 100501(R) (2020); Y. Wang, C.-J. Kang, H. Miao, and G. Kotliar, Hund's metal physics: From SrNiO₂ to LaNiO₂, *ibid.* **102**, 161118(R) (2020).
- [14] M. Kitatani, L. Si, O. Janson, R. Arita, Z. Zhong, and K. Held, Nickelate superconductors—a renaissance of the one-band Hubbard model, *npj Quantum Mater.* **5**, 59 (2020).
- [15] B. H. Goodge, D. Li, K. Lee, M. Osada, B. Y. Wang, G. A. Sawatzky, H. Y. Hwang, and L. F. Kourkoutis, Doping evolution of the Mott-Hubbard landscape in infinite-layer nickelates, *Proc. Natl. Acad. Sci. USA* **118**, e2007683118 (2021).
- [16] S. Ryee, H. Yoon, T. J. Kim, M. Y. Jeong, and M. J. Han, Induced magnetic two-dimensionality by hole doping in the superconducting infinite-layer nickelate Nd_{1-x}Sr_xNiO₂, *Phys. Rev. B* **101**, 064513 (2020).
- [17] S. P. Harvey, B. Y. Wang, J. Fowlie, M. Osada, K. Lee, Y. Lee, D. Li, and H. Y. Hwang, Evidence for nodal superconductivity in infinite-layer nickelates, [arXiv:2201.12971](https://arxiv.org/abs/2201.12971).

- [18] J. Fowlie, M. Hadjimichael, M. M. Martins, D. Li, M. Osada, B. Y. Wang, K. Lee, Y. Lee, Z. Salman, T. Prokscha, J.-M. Triscone, H. Y. Hwang, and A. Suter, Intrinsic magnetism in superconducting infinite-layer nickelates, *Nat. Phys.* **18**, 1043 (2022).
- [19] D. C. Johnston, The puzzle of high temperature superconductivity in layered iron pnictides and chalcogenides, *Adv. Phys.* **59**, 803 (2010); G. R. Stewart, Superconductivity in iron compounds, *Rev. Mod. Phys.* **83**, 1589 (2011); E. Dagotto, *Colloquium: The unexpected properties of alkali metal iron selenide superconductors*, *ibid.* **85**, 849 (2013).
- [20] J. L. Tallon, C. Bernhard, and C. Niedermayer, Muon spin relaxation studies of superconducting cuprates, *Supercond. Sci. Technol.* **10**, A38 (1997).
- [21] A. S. Botana and M. R. Norman, Similarities and Differences between LaNiO_2 and CaCuO_2 and Implications for Superconductivity, *Phys. Rev. X* **10**, 011024 (2020).
- [22] K. W. Lee and W. E. Pickett, Infinite-layer LaNiO_2 : Ni^{1+} is not Cu^{2+} , *Phys. Rev. B* **70**, 165109 (2004).
- [23] C.-J. Kang and G. Kotliar, Optical Properties of the Infinite-Layer $\text{La}_{1-x}\text{Sr}_x\text{NiO}_2$ and Hidden Hund's Physics, *Phys. Rev. Lett.* **126**, 127401 (2021).
- [24] V. I. Anisimov, D. Bukhvalov, and T. M. Rice, Electronic structure of possible nickelate analogs to the cuprates, *Phys. Rev. B* **59**, 7901 (1999).
- [25] J. Karp, A. Hampel, and A. J. Millis, Superconductivity and antiferromagnetism in NdNiO_2 and CaCuO_2 : A cluster DMFT study, *Phys. Rev. B* **105**, 205131 (2022).
- [26] D. Zhao, Y. B. Zhou, Y. Fu, L. Wang, X. F. Zhou, H. Cheng, J. Li, D. W. Song, S. J. Li, B. L. Kang, L. X. Zheng, L. P. Nie, Z. M. Wu, M. Shan, F. H. Yu, J. J. Ying, S. M. Wang, J. W. Mei, T. Wu, and X. H. Chen, Intrinsic Spin Susceptibility and Pseudogaplike Behavior in Infinite-Layer LaNiO_2 , *Phys. Rev. Lett.* **126**, 197001 (2021).
- [27] F. C. Zhang and T. M. Rice, Effective Hamiltonian for the superconducting Cu oxides, *Phys. Rev. B* **37**, 3759 (1988).
- [28] M. Hirayama, Y. Nomura, and R. Arita, *Ab initio* downfolding based on the GW approximation for infinite-layer nickelates, *Front. Phys.* **10**, 824144 (2022).
- [29] M. Hepting, D. Li, C. J. Jia, H. Lu, E. Paris, Y. Tseng, X. Feng, M. Osada, E. Been, Y. Hikita, Y. D. Chuang, Z. Hussain, K. J. Zhou, A. Nag, M. Garcia-Fernandez, M. Rossi, H. Y. Huang, D. J. Huang, Z. X. Shen, T. Schmitt *et al.*, Electronic structure of the parent compound of superconducting infinite-layer nickelates, *Nat. Mater.* **19**, 381 (2020).
- [30] K. Lee, B. Y. Wang, M. Osada, B. H. Goodge, T. C. Wang, Y. Lee, S. Harvey, W. J. Kim, Y. Yu, C. Murthy, S. Raghu, L. F. Kourkoutis, and H. Y. Hwang, Character of the "normal state" of the nickelate superconductors, [arXiv:2203.02580](https://arxiv.org/abs/2203.02580).
- [31] M. Osada, B. Y. Wang, B. H. Goodge, K. Lee, H. Yoon, K. Sakuma, D. Li, M. Miura, L. F. Kourkoutis, and H. Y. Hwang, A superconducting praseodymium nickelate with infinite layer structure, *Nano Lett.* **20**, 5735 (2020).
- [32] X. Ding, S. Shen, H. Leng, M. Xu, Y. Zhao, J. Zhao, X. Sui, X. Wu, H. Xiao, X. Zu, B. Huang, H. Luo, P. Yu, and L. Qiao, Stability of superconducting $\text{Nd}_{0.8}\text{Sr}_{0.2}\text{NiO}_2$ thin films, *Sci. China Phys. Mech. Astron.* **65**, 267411 (2022).
- [33] S. W. Zeng, X. M. Yin, C. J. Li, L. E. Chow, C. S. Tang, K. Han, Z. Huang, Y. Cao, D. Y. Wan, Z. T. Zhang, Z. S. Lim, C. Z. Diao, P. Yang, A. T. S. Wee, S. J. Pennycook, and A. Ariando, Observation of perfect diamagnetism and interfacial effect on the electronic structures in infinite layer $\text{Nd}_{0.8}\text{Sr}_{0.2}\text{NiO}_2$ superconductors, *Nat. Commun.* **13**, 743 (2022).
- [34] P. Choubey and I. Eremin, Electronic theory for scanning tunneling microscopy spectra in infinite-layer nickelate superconductors, *Phys. Rev. B* **104**, 144504 (2021).
- [35] V. Olevano, F. Bernardini, X. Blase, and A. Cano, *Ab initio* many-body GW correlations in the electronic structure of LaNiO_2 , *Phys. Rev. B* **101**, 161102(R) (2020); Q. Gu, Y. Li, S. Wan, H. Li, W. Guo, H. Yang, Q. Li, X. Zhu, X. Pan, Y. Nie, and H.-H. Wen, Single particle tunneling spectrum of superconducting $\text{Nd}_{1-x}\text{Sr}_x\text{NiO}_2$ thin films, *Nat. Commun.* **11**, 6027 (2020).
- [36] G. Kotliar, S. Y. Savrasov, K. Haule, V. S. Oudovenko, O. Parcollet, and C. A. Marianetti, Electronic structure calculations with dynamical mean-field theory, *Rev. Mod. Phys.* **78**, 865 (2006).
- [37] L. Craco, Quantum orbital entanglement: A view from the extended periodic Anderson model, *Phys. Rev. B* **77**, 125122 (2008).
- [38] L. Craco and S. Leoni, Theory of two-fluid metallicity in superconducting FeSe at high pressure, *Phys. Rev. B* **100**, 121101(R) (2019); Mott and pseudogap localization in pressurized NbO_2 , *ibid.* **102**, 045142 (2020).
- [39] For the bare DOS considered in this paper (see Fig. 2), Ref. [[12] online] performed the DFT calculation with the QUANTUM ESPRESSO (QE) [40] computational code. In the DFT calculation, the projector augmented-wave (PAW) pseudopotential was used with the Nd-4f bands being treated as core states. The QE computation was converged with a k -point grid of $16 \times 16 \times 16$ and an energy cutoff of 70 Ry for the wave functions as well as an energy cutoff of 280 Ry for the density and potential. For further details, see Ref. [[12] online].
- [40] P. Giannozzi, S. Baroni, N. Bonini, M. Calandra, R. Car, C. Cavazzoni, D. Ceresoli, G. L. Chiarotti, M. Cococcioni, I. Dabo, A. D. Corso, S. Fabris, G. Fratesi, S. de Gironcoli, R. Gebauer, U. Gerstmann, C. Gougoussis, A. Kokalj, M. Lazzeri, and L. Martin-Samos, QUANTUM ESPRESSO: A modular and open-source software project for quantum simulations of materials, *J. Phys.: Condens. Matter* **21**, 395502 (2009).
- [41] Y. Nomura and R. Arita, Superconductivity in infinite-layer nickelates, *Rep. Prog. Phys.* **85**, 052501 (2022).
- [42] G.-M. Zhang, Y.-F. Yang, and F.-C. Zhang, Self-doped Mott insulator for parent compounds of nickelate superconductors, *Phys. Rev. B* **101**, 020501(R) (2020).
- [43] A. Georges, G. Kotliar, W. Krauth, M. J. Rozenberg, Dynamical mean-field theory of strongly correlated fermion systems and the limit of infinite dimensions, *Rev. Mod. Phys.* **68**, 13 (1996).
- [44] M. Imada, A. Fujimori, and Y. Tokura, Metal-insulator transitions, *Rev. Mod. Phys.* **70**, 1039 (1998).
- [45] A. Droghetti, M. M. Radonjić, A. Halder, I. Rungger, and L. Chioncel, DFT + Σ_2 method for electron correlation effects at transition metal surfaces, *Phys. Rev. B* **105**, 115129 (2022).
- [46] J. Faúndez, T. N. Jorge, and L. Craco, Spin-selective electronic reconstruction in quantum ferromagnets: A view from the spin-asymmetric Hubbard model, *Phys. Rev. B* **97**, 115149 (2018).
- [47] J. L. McChesney, A. Bostwick, T. Ohta, T. Seyller, K. Horn, J. González, and E. Rotenberg, Extended van Hove Singularity

- and Superconducting Instability in Doped Graphene, *Phys. Rev. Lett.* **104**, 136803 (2010).
- [48] A. Liebsch and A. Lichtenstein, Photoemission Quasiparticle Spectra of Sr_2RuO_4 , *Phys. Rev. Lett.* **84**, 1591 (2000).
- [49] S. Link, S. Forti, A. Stöhr, K. Küster, M. Rösner, D. Hirschmeier, C. Chen, J. Avila, M. C. Asensio, A. A. Zakharov, T. O. Wehling, A. I. Lichtenstein, M. I. Katsnelson, and U. Starke, Introducing strong correlation effects into graphene by gadolinium intercalation, *Phys. Rev. B* **100**, 121407(R) (2019); P. Rosenzweig, H. Karakachian, D. Marchenko, K. Küster, and U. Starke, Overdoping Graphene Beyond the van Hove Singularity, *Phys. Rev. Lett.* **125**, 176403 (2020).
- [50] F. Lechermann, Late transition metal oxides with infinite-layer structure: Nickelates versus cuprates, *Phys. Rev. B* **101**, 081110(R) (2020); H. Chen, A. Hampel, J. Karp, F. Lechermann, and A. J. Millis, Dynamical mean field studies of infinite layer nickelates: Physics results and methodological implications, *Front. Phys.* **10**, 835942 (2022).
- [51] K. Limtragoon, C. Setty, Z. Leong, and P. W. Phillips, Realizing infrared power-law liquids in the cuprates from unparticle interactions, *Phys. Rev. B* **94**, 235121 (2016); Z. Leong, C. Setty, K. Limtragoon, and P. W. Phillips, Power-law liquid in cuprate superconductors from fermionic unparticles, *ibid.* **96**, 205101 (2017).
- [52] L. Craco and S. Leoni, Selective orbital reconstruction in tetragonal FeS: A density functional dynamical mean-field theory study, *Sci. Rep.* **7**, 46439 (2017); Orbital selectivity in the normal state of KFe_2Se_2 superconductor, *Europhys. Lett.* **136**, 27002 (2021).
- [53] L. Craco and S. Leoni, Orbital-selective nature of the $3d$ electronic structure of the ThFeAsN superconductor, *Phys. Rev. B* **103**, 075110 (2021).
- [54] P. Werner and A. J. Millis, High-Spin to Low-Spin and Orbital Polarization Transitions in Multiorbital Mott Systems, *Phys. Rev. Lett.* **99**, 126405 (2007).
- [55] Q. Gu and H.-H. Wen, Superconductivity in nickel-based 112 systems, *Innovation* **3**, 100202 (2022).
- [56] L. Craco, M. S. Laad, S. Leoni, and H. Rosner, Theory of the orbital-selective Mott transition in ferromagnetic YTiO_3 under high pressure, *Phys. Rev. B* **77**, 075108 (2008); L. Craco, M. S. Laad, and S. Leoni, Microscopic description of insulator-metal transition in high-pressure oxygen, *Sci. Rep.* **7**, 2632 (2017).
- [57] This choice of parameters gives results for the T dependence of the electrical resistivity which are in good qualitative agreement with experimental data [1,15].
- [58] C. Grenzbach, F. B. Anders, and G. Czycholl, Transport properties of heavy-fermion systems, *Phys. Rev. B* **74**, 195119 (2006).
- [59] L. Craco and M. S. Laad, Normal state incoherent pseudogap in FeSe superconductor, *Eur. Phys. J. B* **89**, 119 (2016).
- [60] Y.-F. Yang and G.-M. Zhang, Self-doping and the Mott-Kondo scenario for infinite-layer nickelate superconductors, *Front. Phys.* **9**, 801236 (2022).
- [61] J. Skolimowski, Y. Gerasimenko, and R. Žitko, Mottness Collapse Without Metallization in the Domain Wall of the Triangular-Lattice Mott Insulator $1T\text{-TaS}_2$, *Phys. Rev. Lett.* **122**, 036802 (2019).
- [62] <http://doi.org/10.17035/d.2022.0219374624>.
- [63] <https://gw4.ac.uk/isambard/>.